Toward High-Power Beam-Steerable Reflectarrays Using Tunable-Height Dielectric

Kendrick Q. Henderson^{ID}, *Member, IEEE*, Walter Disharoon^{ID}, *Graduate Student Member, IEEE*, and Nima Ghalichechian^{ID}, *Senior Member, IEEE*

Abstract— A novel method for a high-power reconfigurable reflectarray (RRA) with a moderate 30° beam scanning is demonstrated. The proposed technique eliminates the need for mechanical steering of reflectors for satellite communication. A small mechanical movement of a patterned dielectric structure under multislot elements achieves beam steering by changing the coupling. Due to the unique shape of the multislot element, the unit cell is capable of tuning the phase for both linear polarization and circular polarization (CP) within a single design operating at 20 GHz. The maximum phase range obtained in this design is a continuous 280° for RHCP, LHCP, and two linear polarizations at 20 GHz. The phase of the reconfigurable unit cell is verified and measured using a waveguide simulator attached to a micromotor. Maximum element loss is simulated to be 0.5 dB. To demonstrate beam steering, three reflectarrays with frozen dielectrics and square array lattices composed of 400 elements ($10\lambda_0 \times 10\lambda_0$) are fabricated. The frozen reflectarrays demonstrate beams at 0°, 15°, and 30°. The measured gain is found to be 23.2 dB at broadside with 21.8 and 23.3 dB, respectively, when scanned to 15° and 30°. The 1 dB gain bandwidth is measured to be 7.45% with a 3 dB axial ratio bandwidth of 12.1%. Unlike other architectures that use nonlinear semiconductor devices, the proposed reflectarray uses a dielectric insert with a height that can be controlled by a micromotor suitable for high-power applications supporting up to 80 MW/m².

Index Terms— Beam steering, mechanical reconfiguration, micromotor, reflectarray.

I. INTRODUCTION

RECONFIGURABLE reflectarrays (RRAs) have distinctive advantages when compared with the standard reflector and phased array antennas [1]. Like a reflector, an RRA exhibits high gain due to its large aperture size.

Kendrick Q. Henderson was with the ElectroScience Laboratory, Department of Electrical and Computer Engineering, The Ohio State University, Columbus, OH 43212 USA. He is now with the NSWC–Crane Division, Crane, IN 47522 USA (e-mail: kendrick.q.henderson.civ@us.navy.mil).

Walter Disharoon is with the School of Electrical and Computer Engineering, Georgia Institute of Technology, Atlanta, GA 30308 USA (e-mail: wdisharoon3@gatech.edu).

Nima Ghalichechian is with the School of Electrical and Computer Engineering, Georgia Institute of Technology, Atlanta, GA 30308 USA (e-mail: nima.1@gatech.edu).

Similar to a phased array, RRA has beam-shaping and beam-steering capabilities as every element within the array acts as a phase shifter to the incident wave from the feed horn. However, unlike a phased array which requires a complex and expensive electronic circuit for each element, an RRA is fed by a single horn antenna. Given the simplicity of feeding architecture, RRAs are an excellent candidate for radar and communication applications. A key challenge for the realization of successful RRA, nonetheless, is the implementation of the phase-shifting elements across the aperture.

Recent advancements in RRAs have increased the bandwidth and aperture efficiency through the use of active elements such as p-i-n and varactor diodes [2], [3], [4], [5], [6], [7]. Various techniques, such as antenna–filter–antenna, which were previously used to create wideband frequency selective surfaces and transmitarrays (i.e., lenses), have been recently employed to make reflectarrays [8], [9], [10]. Diode designs using the aforementioned technique and split patch antennas can have aperture efficiencies up to 15% and 1 dB gain bandwidth of up to 8%. However, such RRAs have insufficient power handling capacity as they exhibit nonlinear behavior when exposed to high-power levels that are found in radar applications [11]. Therefore, an RRA that can handle relatively high-power levels is desirable for transmit applications.

As compared to nonlinear semiconductor-based approaches (e.g., p-i-n diode), a mechanically reconfigured reflectarray has the ability to handle much higher power levels albeit with a slower reconfiguration speed. With the current commercially available piezoelectric or stepper motor actuators and relays, it is possible to design a mechanically RRA that can handle high-power levels with a wide bandwidth to replace both reflector antennas and phased arrays in certain applications [12], [13], [14]. In our design, by not including a lossy active device in the path of the configured field, mechanical reconfiguration allows the RRA unit cell to stay passive.

Circular polarization (CP) has the benefit of allowing random orientation between cellular base stations and the user equipment or satellites and ground terminals. For reflectarrays to be used in these areas, the arrays need to be capable of CP. As an example, a unique method proposed by [15] uses microactuators to tilt a resonate surface of square patches to steer the illumination from a feed horn. Unfortunately, the peak gain of the antenna is that of the feed horn since the patches

are not creating a collimated wavefront. The patches are only reducing the necessary tilt angle that would be needed with a nonresonate reflective surface such as a sheet of copper.

One method for creating CP RRAs with a collimated wavefront is to create a rotating dual-ring resonator [14]. Although the rotation of the unit cell by a micromotor does provide a continuous phase response of 360°, it is limited to only CP. Another method involves the use of a slotted patch that is coupled to a radiating patch antenna [16]. A micromotor that controls the gap distance varies the coupling between the two patches. While the unit cell has a large phase range of 324° and the reflectarray has a scanning range of 60°, it cannot withstand high-power due to the small gap between the two patches as it leads to field enhancement. The design of [12] and [13] can withstand higher power levels due to the aluminum casing and the care taken to reduce the field enhancement via a circular patch. However, the integrated relays for reconfiguration in the RRA yield only the two phase states of 0° and 180°.

There are examples of mechanically reconfigurable transmitarray antennas [17], [18]. Unfortunately, these antennas do not report high power capability. A similar example in the lens does report power handling capability [19] but has very poor radiation efficiency and small bandwidth. We expect this type of design would have the benefit of no feed blockage and comparable amplitude and phase capabilities. However, these methods may suffer at high-powers from having the reconfigurable device not shielded by a ground plane and the reflected power now returns toward the feed.

Recently, we pursued several methods for antenna and array reconfigurations in our research group. Examples include a W-band frequency reconfigurable slot antenna using paraffin phase change material [20], [21], mechanically reconfigured slot array using accordion-like microactuators [22], electrically reconfigured millimeter wave sensors [23], [24], and reflectar-rays [25] using vanadium dioxide phase change material.

In this article, we build on our latest examination of circularly polarized multislot reflectarray antennas [26] and the study of rectangular and triangular lattices for beam shaping [27]. We demonstrate a continuously and mechanically reconfigured unit cell that varies the height of a dielectric to change the capacitance inside a uniquely designed multislot element. Fig. 1 illustrates the schematic design with the multislot dielectric and the method of reconfiguration. The unique features are the ability to handle a high peak power and polarization diversity of the design. The concept of the dielectric to reconfigure the multislot was presented in our preliminary design [28]. For this work, however, a 3-D-printed material is used as the dielectric under the metallic aperture. In our work, we demonstrate the fabrication and testing of a fully reconfigurable unit cell using a micromotor and a waveguide.

Full reconfiguration of an array with 400 elements, however, is very challenging. Instead, to demonstrate the concept of the dielectric reconfiguration method in an array environment, the reflectarray is designed as three separate *frozen* prototypes. A similar approach was reported in the past for several RRAs [29], [30], [31], [32]. To further validate beam steering
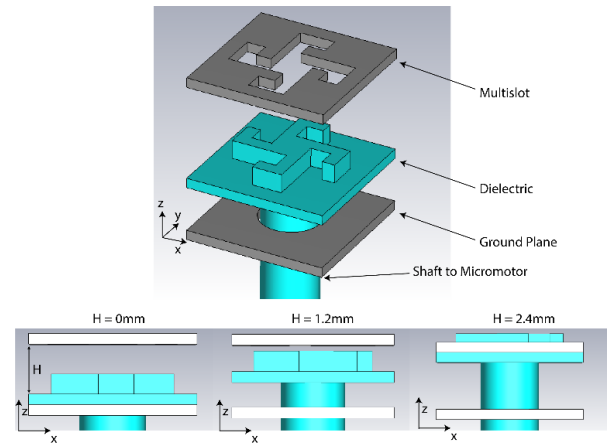

Fig. 1.   Proposed high-power RRA unit cell. The design consists of the stainless-steel multislot, dielectric for reconfiguration, and stainless-steel ground plane with an opening for the shaft. The shaft moves the dielectric from the ground plane toward the multislot.

with a micromotor (instead of the *frozen* design), we designed and measured a reconfigurable waveguide-based unit cell. This article is structured as the following. We discuss the unit cell design, waveguide-based prototype, micromotor-controlled reflectarray concept, comparison of the fully reconfigured array versus *frozen* design, and power handling in Section II. Full-wave simulation setup and results for a reflectarray with 400 elements are discussed in Section III. The fabrication and measurement results are reported in Section IV. This article is concluded in Section V.

II. REFLECTARRAY UNIT CELL

A. Unit Cell Design and Simulation

The proposed RRA unit cell in Fig. 1 is a modified version of our previous design in which the low-loss multislot element exhibited 360° of phase range with four L-shaped slots of varying lengths with a square slot element [26]. The unique feature of this design is CP with a low axial ratio achieved by a metal-only architecture. In the new proposed unit cell, however, the multislot is instead fixed in shape and size while the dielectric is moved inside of the slot by a micromotor. Unlike other mechanically reconfigured reflectors that occupy a large space when steered, the proposed RRA has a fixed counter. This is because only the geometry between the top plate and the ground plane is changing. This continuous capacitance change is then used to tune the reflected phase of the now reconfigurable unit cell. Detailed geometry of the multislot and the dielectric is shown in Fig. 2.

The unit cell consists of three parts: 1) the multislot laser-etched into a 0.52 mm thick stainless-steel layer; 2) the 3-D-printed dielectric (VeroWhite Plus with $\varepsilon_r = 2.75$, tan $\delta = 0.02$ [33], [34]) to configure the phase; and 3) the 0.52 mm thick stainless-steel ground plane with a hole for the shaft of the dielectric that connects to the micromotor. The design geometry of the multislot operating at 20 GHz is listed in Fig. 2(b). The dielectric dimensions, listed in Fig. 2(a), are identical to the multislot but reduced by 0.3 mm
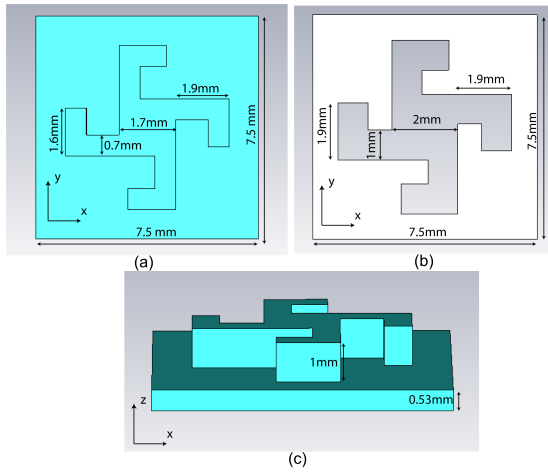
Fig. 2. Schematic of the multislot element showing the dimensions of (a) multislot, (b) 3-D-printed dielectric insert, and (c) side view of the dielectric insert where insertion and base heights are 1 and 0.53 mm, respectively.
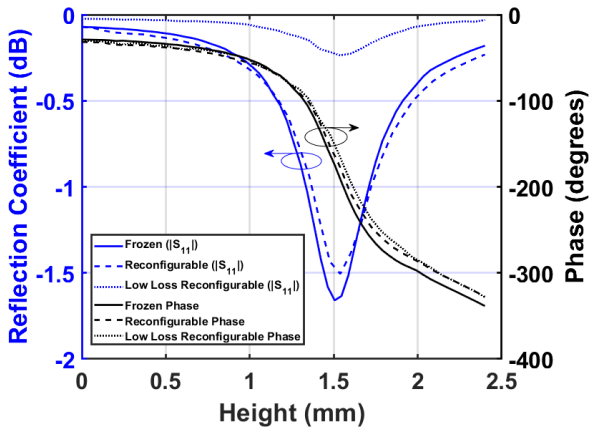

Fig. 3. Amplitude and phase of the reflected field as a function of dielectric height at 20 GHz. A phase range of 280° is achieved. The two phase plots overlap enabling operation in four polarizations achieved via a unique unit cell design.
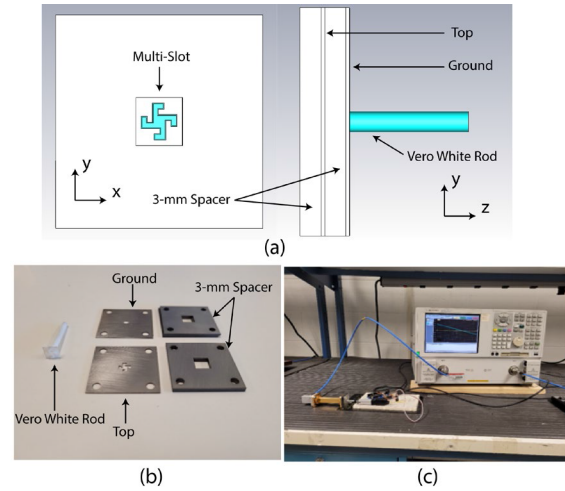

Fig. 4. (a) Top- and side-view schematic of the reconfigurable unit cell with WR-51 waveguide. (b) Fabricated unit cell (without the waveguide) for phase measurement. (c) Unit cell and the waveguide are connected to a VNA for phase measurements.

in size to allow the fabrication tolerances. The distance between the multislot and the ground plane is fixed at 3 mm ($\lambda_0/5$). The base of the dielectric [illustrated in Fig. 2(c)] is 0.53 mm for the reconfigurable unit cell.

CST Microwave Studio is used to determine the element's magnitude and phase response. First, the unit cell is simulated using periodic boundary conditions and a Floquet port for excitation. The movement of the dielectric from the ground plane toward the multislot, as illustrated in Fig. 1, increases the capacitance between the slots. The dielectric has a displacement range of 2.4 mm. The change in capacitance is employed to tune the reflection phase. The total reflection phase of the unit cell, shown in Fig. 3, is 280°, which is expected to increase the quantization as well as scan losses [35]. One unique feature of this cell is that it can change the phase of two linear polarizations and two CPs, with the phase response for each of these polarizations remaining the same. The magnitude of the reflection coefficient for the unit cell is also of interest as it shows the losses associated with each element. Fig. 3 (left axis) illustrates that loss of the unit

cell with a low loss dielectric ($\varepsilon_r = 2.75$, $\tan \delta = 0.002$) and copper conductor is below 0.5 dB. A higher loss dielectric and stainless steel are used in this initial work to reduce fabrication complexity.

B. Waveguide-Based Prototype

To verify the phase response of the reconfigurable unit cell with a micromotor, a waveguide *emulator* (prototype) is implemented. To mimic an infinite array environment, an image current is needed at the unit cell's boundaries. This is achieved by using metal (stainless-steel) walls that surround the unit cell as shown in Fig. 4. The unit cell can fit inside the short walls of the WR-51 waveguide with a frequency range of 15–22 GHz. To set up the image of the unit cell, a 3 mm thick stainless-steel section is placed above the cell with a $0.5\lambda_0 \times 0.5\lambda_0$ ($\lambda_0 = 15$ mm) cut at its center. Another steel section is placed between the top metal and the ground plane on each side. Fig. 4(a) shows the modified unit cell placed inside the waveguide. After full-wave modeling, the unit cell is fabricated as shown in Fig. 4(b). The stainless-steel pieces were fabricated using a laser etching process. The process had a tolerance of 0.024 mm or 0.001 in. Due to fabrication restraints, the two 3 mm pieces of steel with the $0.5\lambda_0 \times 0.5\lambda_0$ slot had to be made from two 1.5 mm pieces. To fabricate the dielectric that tunes the phase of the multislot, a 3-D printing process (PolyJet with VeroWhite Plus material) is used. The process has a lateral resolution tolerance of 0.043 mm and a height resolution of 16 μm. The unit cell is fabricated and connected to a WR-51 waveguide and a micromotor [Fig. 4(c)].

To control the movement of the dielectric inside of the unit cell, a linear stepper motor (L12-30-50-6-R) is used with 0.1 mm ($\lambda_0/150$) step resolution. The simulation and measurement results of the waveguide simulator are both shown in Fig. 5. The fabricated unit cell shows good agreement with the simulated waveguide results for phase. The amplitude performs worse due to the resonance introduced by the poor
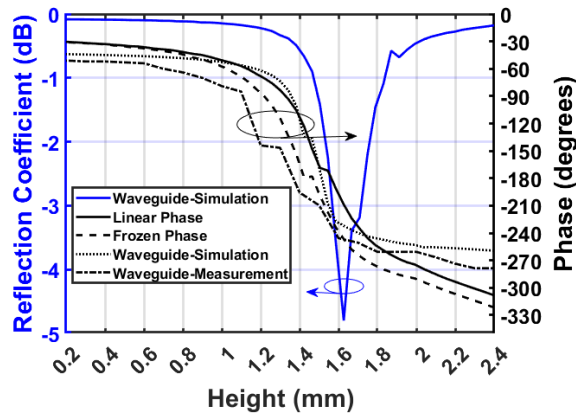
Fig. 5. Measured and simulated phases of the reflected field as a function of dielectric height at 20 GHz for the unit cell using a waveguide prototype. The results are compared with the periodic boundary condition cases.
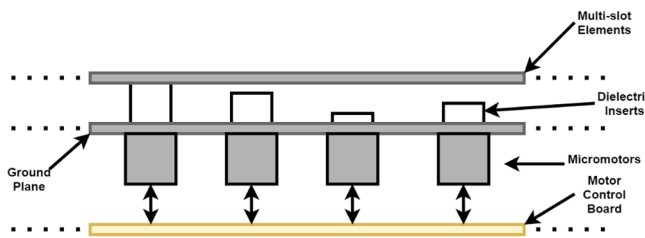

Fig. 6. Block diagram of the proposed motor and control board integration.

Fig. 7. Example block diagram of the proposed integration of the motor controllers, FPGAs, and microcontroller.

fitting of the waveguide relative to the unit cell. The waveguide aperture was smaller than the unit cell vertically and larger horizontally. The waveguide simulator validates the capability of the reconfigurable unit cell's phase response as a function of the dielectric's displacement.

C. Micromotor Controlled Reflectarray

The development of a control board and its circuitry would allow for the full integration of the motors below the reflectarray's aperture. The proposed diagram of the integration is shown in Fig. 6. The design of the control circuitry would have to include the same number of motor controllers as unit cells in the controlled reflectarray. The motor controllers are necessary to apply the correct excitation to the motors and to track the position of the shafts. The input and output of the motor controllers would be managed by a series of field programmable gate arrays (FPGAs). Finally, the FPGAs would be managed by microcontrollers that would apply the correct phase response across the reflectarray's aperture. The proposed circuit is shown in Fig. 7. The reconfiguration speed is expected to be limited by the mechanical movement of the motor. In our design, the expected full range of motion is achieved in less than 94 ms.

D. Frozen Design Cell

To test the ability of the unit cell to form and steer the beam in a reflectarray, while avoiding the cost and complexity of the array with 400 micromotors, the unit cell is made into three *frozen* designs illustrated in Fig. 8. Here, the dielectric height is fixed during fabrication instead of implementing
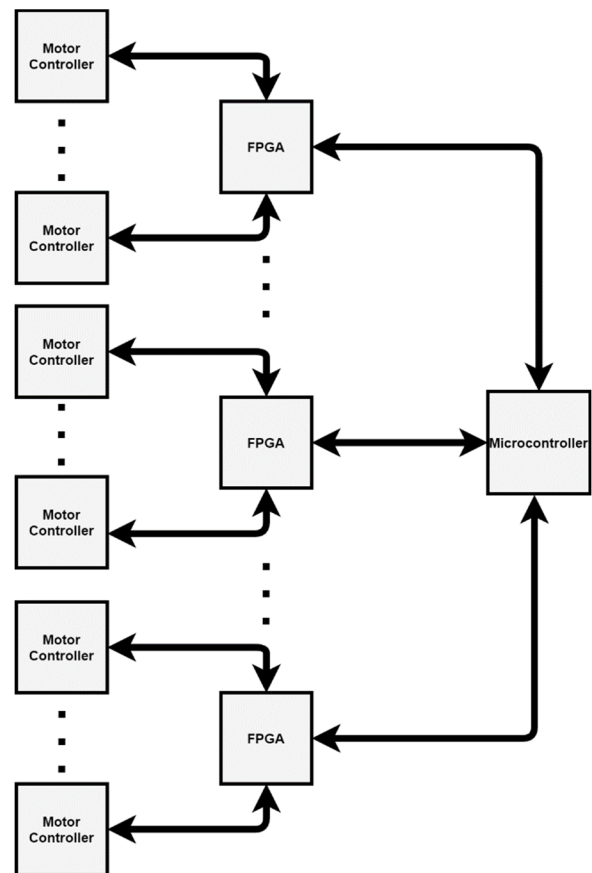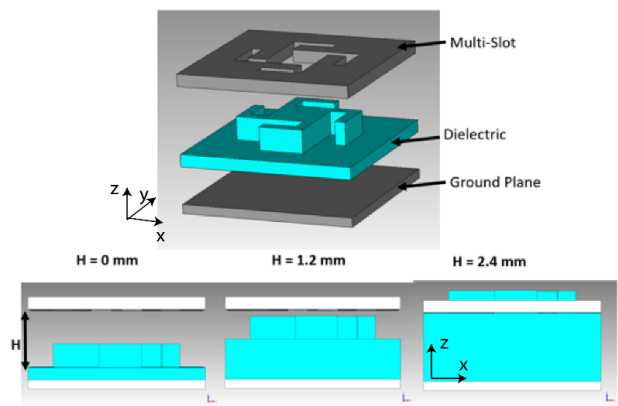

Fig. 8. Frozen high-power RRA unit cell (modified version of Fig. 1). The design consists of the stainless-steel multislot, ground plane, and 3-D printed dielectric. The thickness of the dielectric is increased to move it toward the multislot.

micromotors beneath the ground plane. The design has the same 2.4 mm displacement range. The phase response range of the fixed unit cell (Fig. 8) is 300° as compared with 280° for the fully reconfigurable design (Fig. 1).

The key difference between the micromotor and *frozen* designs is that, in the latter, the dielectric can completely fill the space between the multislot and the ground plane. The fixed design has a resonant frequency shift as a result of the additional dielectric material. Nevertheless, as illustrated
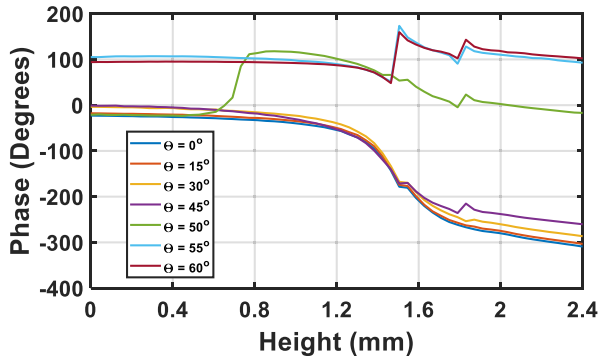
Fig. 9. Phase response of the reconfigurable unit cell as a function of incident angle. The phase response of the unit cell is similar until an incident angle of 50°.

Fig. 10. Side view of the reconfigurable reflectarray unit cell showing the E-field at 20 GHz (0° incident). Only the fundamental mode propagates in the unit cell at an incident angle of 0°. The profile of the E-field is shown at (a) 0° and (b) 90° phase. The dielectric was placed at peak height.

Fig. 11. Side view of the reconfigurable reflectarray unit cell showing the E-field at 20 GHz (45° incident). A guided wave propagates in the unit cell at an incident angle of 45°. The profile of the E-field is shown at (a) 0° and (b) 90° phase. The dielectrics were placed at peak height.

in Fig. 3, the shape of the response between the two unit cells is similar. Therefore, for validation of the reflectarray's parameters and simplicity, we demonstrate the fabrication and testing results of the *frozen* reflectarray in Section IV.

E. Fully Reconfigurable Versus Frozen

The sensitivity to incident angles for: 1) the fully reconfigurable unit cell (as shown in Fig. 1) and 2) the *frozen* design (as shown in Fig. 8) is investigated. This study provides insight into the array steering limitation. The phase response as a function of incident angle and the dielectric height for the fully reconfigurable array is shown in Fig. 9. To further determine the root cause for scan angle limitation, the simulated E-field contours for 0° and 45° incident waves are shown in Figs. 10 and 11, respectively. The phase response as a function of incident angle and the dielectric height for the *frozen* array is shown in Fig. 12 followed by E-fields for 0° and 30° incident waves in Figs. 13 and 14, respectively. The fully reconfigurable unit cell has a consistent phase response up to the incident angle of 50°. At this angle, the phase response begins to rise at a dielectric displacement height of 0.6 mm. This limits the scanning range of the reflectarray to less than 50° as it distorts the radiation pattern. The *frozen* unit cell has a similar phase response until an incident angle of 30° at a dielectric displacement height of 0.6 mm. The cause of the phase distortion in both unit cells is the propagation of a guided wave between the two stainless-steel layers. This wave is instigated by the presence of the dielectric layer as it was not present in our previous metal-only reflectarrays with air as a dielectric [26], [27]. Thus, the dielectric causes a phase delay across the unit cell's aperture at these incident angles which results in the guided wave's formation and propagation. Since Fig. 11 shows the fully reconfigurable unit cell below the critical angle of 50°, the formation of the guided wave can be seen as the phase progresses. Fig. 14 illustrates the 30° critical limit for the frozen unit cell. The guided wave can be seen propagating as the phase progresses. Based on the above simulation results, we conclude that while the *frozen* design is simpler to fabricate and study, its steering capability is inferior and is only limited to ±30°.
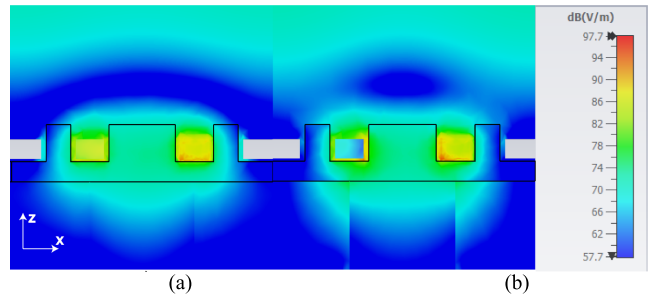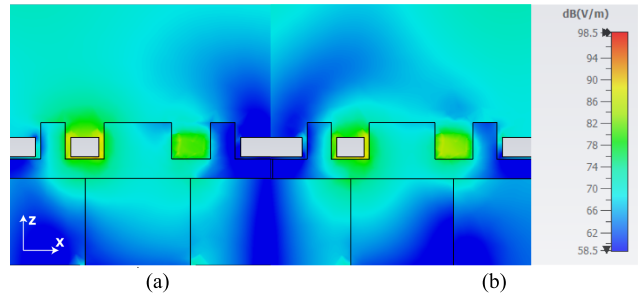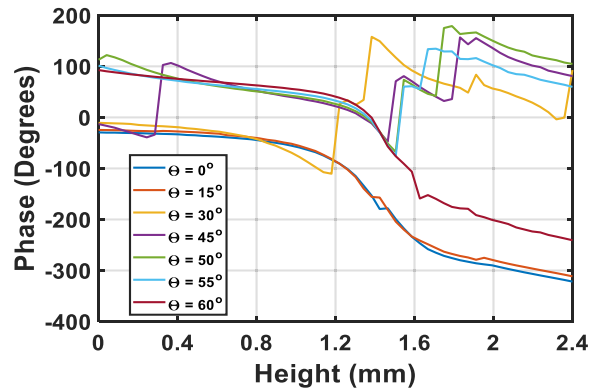

Fig. 12. Phase response of the frozen unit cell as a function of incident angle. The phase response of the unit cell is similar until an incident angle of 30°. The additional dielectric material further limits the phase response to larger incident angles.

F. Power Handling Study

To validate the high peak power capability of the unit cell for arrays, the electric field distribution is simulated. Hence, the peak power limit is calculated using the maximum field of the element, the breakdown strength of air (3 MV/m), and the simulated input power of 0.5 W. By examining Fig. 15, the maximum electric field of the element is 31.5 kV/m resulting in a peak power capacity of 4.51 kW per element from the following:

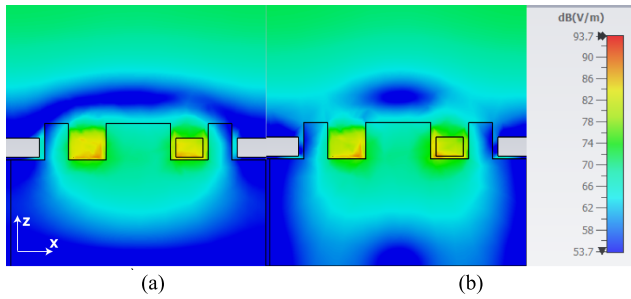$$\frac{P_b}{P_i} = \left(\frac{E_b}{E_i}\right)^2 \tag{1}$$

Fig. 13. Side view of the frozen reflectarray unit cell showing the E-field at 20 GHz. Only the fundamental mode is excited in the unit cell at an incident angle of 0°. The profile of the E-field is shown at (a) 0° and (b) 90° phase. The dielectric was placed at peak height.
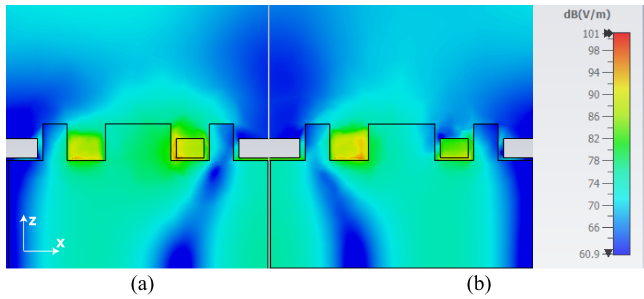

Fig. 14. Side-view of the frozen reflectarray unit cell showing the E-field at 20 GHz. A guided wave propagates in the unit cell at an incident angle of 30°. The profile of the E-field is shown at (a) 0° and (b) 90° phase. The dielectric was placed at peak height.
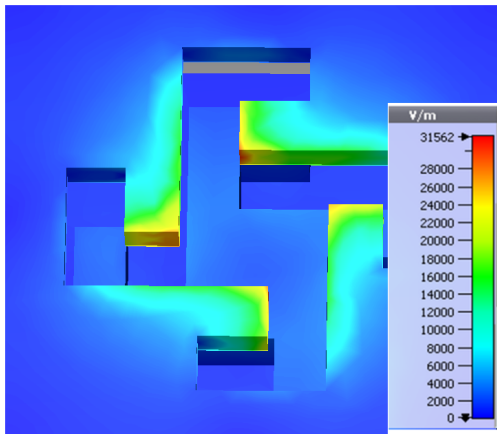

Fig. 15. Electric field distribution of the multislot element at minimum dielectric height. The peak electric field is 31.5 kV/m.
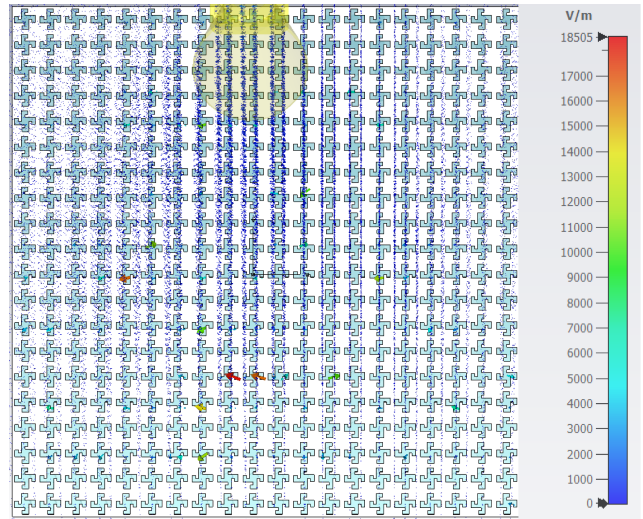

Fig. 16. Electric field distribution on the finite reconfigurable array. The red arrows signify locations where the field is reaching the peak.
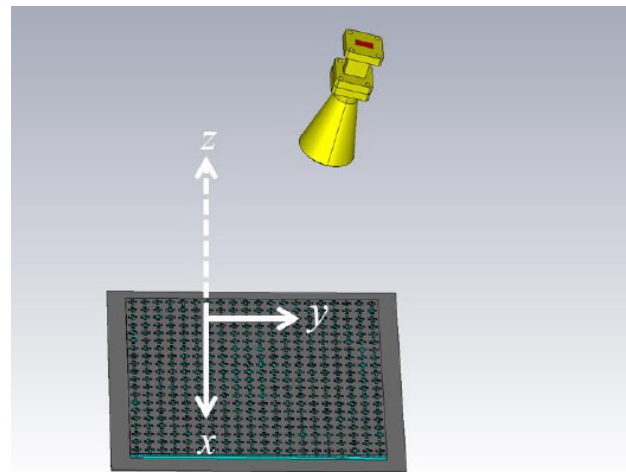

Fig. 17. CST Studio Suite model of the reflectarray design. The model consists of 400 elements and the feed horn. Scanning is performed in the y–z plane.

where P_b and P_i are defined as the power before breakdown and the simulated input power, respectively.

For a uniformly illuminated reflectarray, this would result in a peak power of 80 MW/m² at 20 GHz. We note that we only considered dielectric breakdown voltage in a uniform array for establishing the power limits. As such, other secondary effects such as the thermal budget are not taken into consideration in our study. A complete power handling of the array can be found by looking at the feed location, illumination taper, and temperature effects from the average power of the target application. For instance, the full-wave simulation of the finite reconfigurable array shown in Fig. 16 does not have a desirable

feed placement or illumination taper. Therefore, the peak input power is limited to 13 kW. The design successfully achieves the two objectives of this work: 1) high peak power capability and 2) supporting four polarizations (RHCP, LHCP, and two linear polarizations).

III. FULL-WAVE SIMULATION OF REFLECTARRAY

The Integral Solver (CST Studio Suite) is used to model and design several *frozen* RRAs. The reflectarray is simulated for beam steering, steering limitation, gain bandwidth, and polarization purity. Fig. 17 illustrates the position of the horn with respect to the array. The square reflectarray is designed as $10\lambda_0 \times 10\lambda_0$, which is excited using a K-band conical horn (Eravant SAC-1533-470-S2) with a 30° half-power beamwidth. The horn supports both linear polarizations and CPs. To maximize the efficiency and avoid feed blockage, the feed horn is placed at a focal length ratio of 1 and at an offset angle of 25°. To create the CPs, two linear polarizations
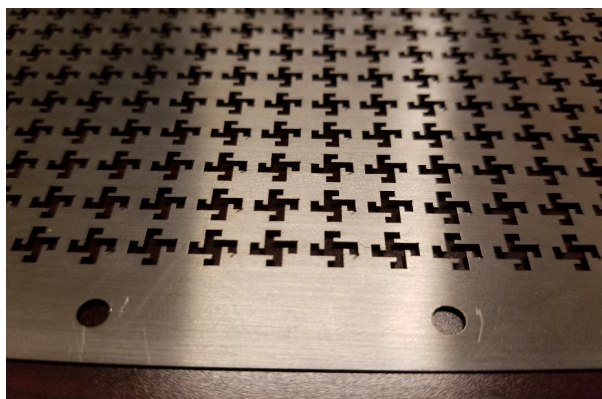
Fig. 18. Multislot elements laser-etched into a stainless-steel sheet. No significant fabrication defects were noticed in the elements.
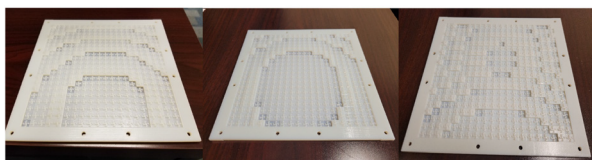
Fig. 19. Three 3-D-printed dielectrics for the frozen reflectarray. From left to right, the dielectrics correspond to 0°, 15°, and 30°, respectively.

are simulated and then combined in post-processing in CST with the appropriate 90° phase shift.

IV. FABRICATION AND MEASUREMENT

Three *frozen* designs were fabricated and measured to verify the reflectarray's parameters. Fig. 18 shows the fabricated stainless-steel layer (common aperture) that contains the multislot of the unit cell. Stainless steel is chosen for ease of fabrication and can be replaced or electroplated in the future with a better-conducting material such as copper. The 0.52 mm thick stainless-steel layer is fabricated using the same laser etch process for waveguide prototype (discussed in Section II-B). To assemble the array, a series of mounting holes were drilled along the exterior of the reflectarray. Fig. 19 shows the fabricated dielectrics for three beams located at 0°, 15°, and 30° along the $y-z$ plane of the reflectarray. The orientation of the array was previously shown in Fig. 17.

A rotator plate is then fabricated to mount the reflectarray in the anechoic chamber. This plate, which is used for mechanical support and testing purposes behind the ground plane, exhibited no adverse effect on the electromagnetic performance. The rotator plate is also used to secure the 3-D-printed feed assembly in the proper position. An orthomode transducer (model # SAT-FK-42042-S1, Sage Millimeter Inc.) is attached to the feed horn to separately excite both vertical and horizontal polarizations. This transducer facilitates testing of the reflectarray without the need to rotate the feed horn during gain measurements, avoiding spatial or angular errors, hence eliminating an important source of measurement error. The orthomode transducer does introduce a loss of 0.5 dB for each linear polarization.

Three reflectarrays were then tested in the anechoic chamber for three beam positions as shown in Fig. 20. Gain patterns for
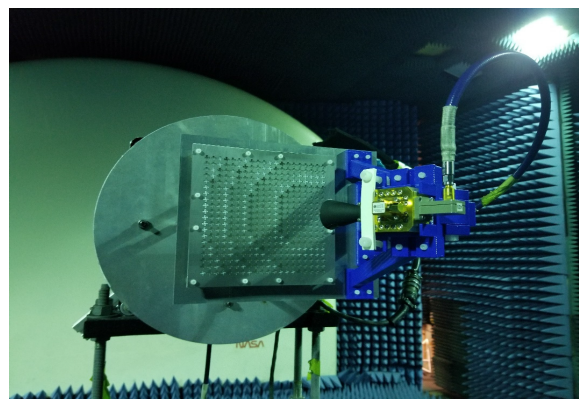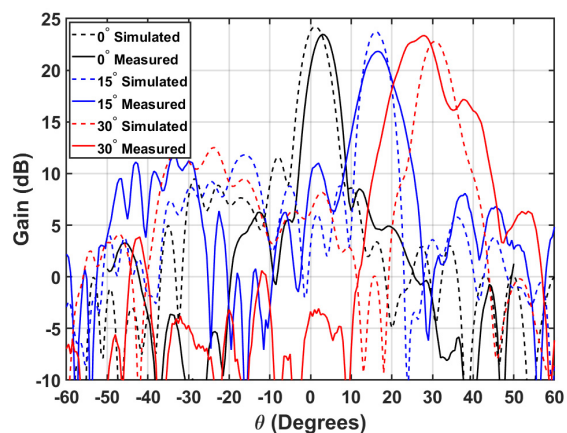

Fig. 20. Measurement setup for the reflectarray (multislot metallic surface, dielectric layer, ground plane, rotator plate, and the feed horn) mounted in the anechoic chamber.

Fig. 21. Measured and simulated radiation patterns for the RHCP at 20 GHz scanned at 0°, 15°, and 30° in the $y-z$ plane. The measured peaks are at 3°, 16.5°, and 28°, respectively.

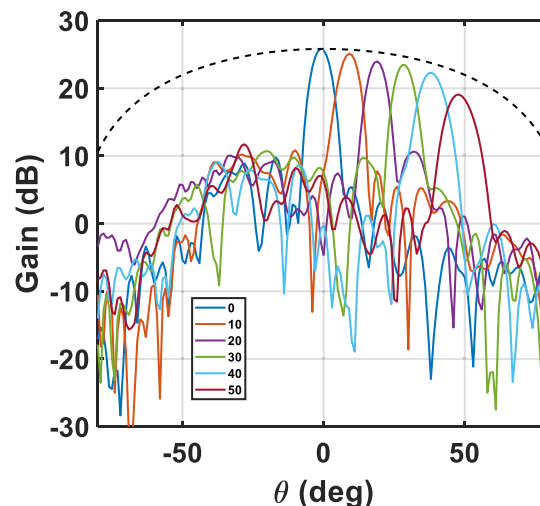Fig. 22. Simulated radiation patterns for LHCP in the $y-z$ plane at 20 GHz scanned at 0°, 10°, 20°, 30°, 40°, and 50°.

the three dielectrics and beam positions are shown in Fig. 21. The simulated gain patterns for the reconfigurable array for six beam positions are illustrated in Fig. 22. The reconfigurable design had a peak simulated gain of 25.8 dB at broadside.
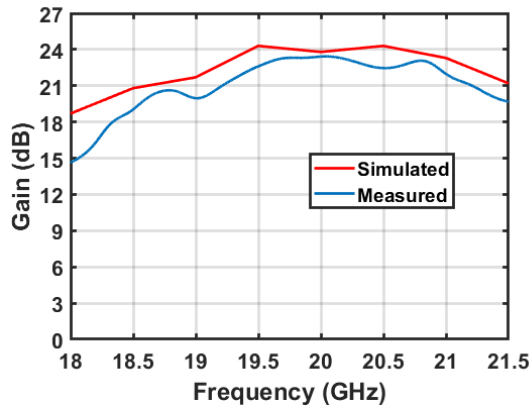
Fig. 23. Simulated and measured gain-bandwidth of the reflectarray for a pattern normal to the surface. The array is designed to operate at 20 GHz.
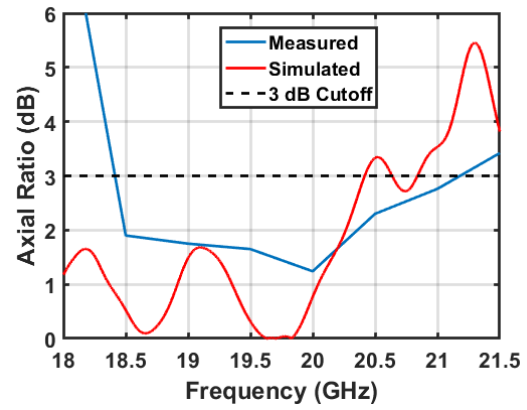

Fig. 24. Simulated and measured axial ratio of the reflectarray for a pattern normal to the surface. The array is designed to operate at 20 GHz.

The frozen antenna exhibited the maximum simulated gain of 24 dB at broadside, 23.7 dB at 15°, and 22.8 dB at 30°. To test its scanning capability, the beam is steered from 0° to 15°, and 30° in the *y–z* plane (in the plane of the feed horn) using three *frozen* designs. The measured gain is 23.2, 21.8, and 23.3 dB, respectively, at 3°, 15°, and 30°. The rise in gain at 30° is due to the spectral reflection of the feed horn. As seen here, a coma lobe does develop at 30° because the unit cell does not have a wide-angle phase response discussed earlier in Section II-E. Effectively, a guided wave begins to propagate in the reflectarray at 30°. The measured sidelobe levels are −13.9 dB when scanned to 0° and −10 dB when scanned to 15°. The scan resolution of the reflectarray is 3.9° based on the $0.5\lambda_0$ spacing of the elements, the 300° phase range (see Fig. 5 and Section II-C), and the 0.1 mm step resolution of the micromotor. The scan resolution is calculated by looking at the array factor with the minimum progressive phase shift, β, to find the minimum steering angle

$$\beta = \frac{\text{Phase Range}}{\text{Motor Range}}(\text{Step Resolution}). \qquad (2)$$

The simulated and measured aperture efficiencies (at broadside) are 20% and 16.6%, respectively. The efficiency can be improved by replacing stainless steel with copper and VeroWhite layer with a low-loss dielectric substrate. When simulated, a 6% improvement in efficiency with the low-loss dielectric ($\epsilon_r = 2.75$, $\tan\delta = 0.002$) and copper is observed. The aperture efficiency of the simulated reconfigurable array (at broadside) is 30.4%. Our material choice was based on the ease of fabrication and costs and was not driven by the efficiency. The gain bandwidth (for both circular and linear polarizations) is shown in Fig. 23. The simulated and measured 1 dB bandwidths were 8.75% and 7.45%, respectively. On average, the measured gain was 1.5 dB less than the simulated gain. The measured value was less than the simulated gain due to the 0.5 dB loss from the orthomode transducer, the difference in the loss tangent of the VeroWhite in each case and the stainless-steel alloy conductivity that was used in the fabrication of the aperture. The parameters differ because VeroWhite is not a well-characterized material for RF applications and the stainless steel alloy used was

TABLE I
COMPARISON BETWEEN VARIOUS RRAS AND RTAS

Parameter	This Work	[14]	[16]	[17]
Frequency (GHz)	20	8	4.8	20
Aperture Efficiency (%)	16.6	51.8	48.6	22
1 dB BW (%)	7.45	28.60	6.20	~2.0
Steerable Range (°)	30	60	60	40
Gain (dB)	23.2	25.6	25.7	30.9
Array Size ($\lambda \times \lambda$)	10 × 10	7.5×7.5	8.5 × 8.5	23×23
Array Shape	Square	Square	Circular	Circular
Polarization	LHCP, RHCP, and LP	LHCP	LP	RHCP, LHCP
Power Handling	80 MW/m²	N/A	N/A	N/A

not characterized. Therefore, common stainless was used in the simulation. We note that we used stainless steel instead of copper as the laser etching process works better for this material. Fig. 24 shows the axial ratio as a function of frequency. The measured axial ratio demonstrated excellent performance (<2 dB for 18–20.5 GHz). The simulated and measured axial ratio bandwidths were 13.9% and 12.1%, respectively. We note that these are both larger than gain bandwidth. The measured results exhibit good agreement with the simulation, especially at the designed frequency of 20 GHz.

V. CONCLUSION

A novel mechanically reconfigured RRA unit cell using a tunable-height dielectric is presented as an alternative to nonlinear and conventional p-i-n and varactor diodes. A comparison table between this work and existing mechanical RRAs and transmitarrays is shown in Table I.

The validation is performed at several levels. First, using a waveguide prototype with a micromotor, the reconfigurability is illustrated and measured. Second, to validate the larger array performance, three *frozen* versions of the reflectarray are fabricated with fixed dielectric heights. Since the difference
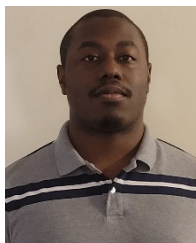
between the *frozen* and fully reconfigurable unit cell is a minute frequency shift, this work can be extended into a fully RRAs. The current design does have a limited field of view because of the dielectric insert. In contrast to other RRAs that use semiconductor devices exhibiting nonlinear (power) behavior, the demonstrated array employs mechanical reconfiguration between the aperture and the ground plane. The potential impact of this work is on high-power RRA with a moderate scanning of 30° frozen and 50° reconfigurable, which is capable of steering linear polarization and CP.

REFERENCES

[1] S. V. Hum and J. Perruisseau-Carrier, "Reconfigurable reflectarrays and array lenses for dynamic antenna beam control: A review," *IEEE Trans. Antennas Propag.*, vol. 62, no. 1, pp. 183–198, Jan. 2014, doi: 10.1109/TAP.2013.2287296.

[2] J. Han, L. Li, G. Liu, Z. Wu, and Y. Shi, "A wideband 1 bit 12×12 reconfigurable beam-scanning reflectarray: Design, fabrication, and measurement," *IEEE Antennas Wireless Propag. Lett.*, vol. 18, no. 6, pp. 1268–1272, Jun. 2019, doi: 10.1109/LAWP.2019.2914399.

[3] S. Costanzo, F. Venneri, A. Raffo, G. Di Massa, and P. Corsonello, "Radial-shaped single varactor-tuned phasing line for active reflectarrays," *IEEE Trans. Antennas Propag.*, vol. 64, no. 7, pp. 3254–3259, Jul. 2016, doi: 10.1109/TAP.2016.2562673.

[4] M. T. Zhang et al., "Design of novel reconfigurable reflectarrays with single-bit phase resolution for Ku-band satellite antenna applications," *IEEE Trans. Antennas Propag.*, vol. 64, no. 5, pp. 1634–1641, May 2016, doi: 10.1109/TAP.2016.2535166.

[5] M. E. Trampler and X. Gong, "Phase-agile dual-resonance single linearly polarized antenna element for reconfigurable reflectarray applications," *IEEE Trans. Antennas Propag.*, vol. 67, no. 6, pp. 3752–3761, Jun. 2019, doi: 10.1109/TAP.2019.2908041.

[6] A. Clemente, F. Diaby, L. D. Palma, L. Dussopt, and R. Sauleau, "Experimental validation of a 2-bit reconfigurable unit-cell for transmitarrays at Ka-band," *IEEE Access*, vol. 8, pp. 114991–114997, 2020, doi: 10.1109/ACCESS.2020.3003698.

[7] H. Yang, F. Yang, S. Xu, M. Li, X. Cao, and J. Gao, "A 1-bit multipolarization reflectarray element for reconfigurable large-aperture antennas," *IEEE Antennas Wireless Propag. Lett.*, vol. 16, pp. 581–584, 2016, doi: 10.1109/LAWP.2016.2590478.

[8] A. Abbaspour-Tamijani, K. Sarabandi, and G. M. Rebeiz, "Antenna-filter-antenna arrays as a class of bandpass frequency-selective surfaces," *IEEE Trans. Microw. Theory Techn.*, vol. 52, no. 8, pp. 1781–1789, Aug. 2004, doi: 10.1109/TMTT.2004.831572.

[9] Y. Li, L. Li, Y. Zhang, and C. Zhao, "Design and synthesis of multilayer frequency selective surface based on antenna-filter-antenna using Minkowski fractal structures," *IEEE Trans. Antennas Propag.*, vol. 63, no. 1, pp. 133–141, Jan. 2015, doi: 10.1109/TAP.2014.2367523.

[10] P. Naseri, F. Khosravi, and P. Mousavi, "Antenna-filter-antenna-based transmit-array for circular polarization application," *IEEE Antennas Wireless Propag. Lett.*, vol. 16, pp. 1389–1392, 2017, doi: 10.1109/LAWP.2016.2638469.

[11] S. V. Hum, M. Okoniewski, and R. J. Davies, "Modeling and design of electronically tunable reflectarrays," *IEEE Trans. Antennas Propag.*, vol. 55, no. 8, pp. 2200–2210, Aug. 2007, doi: 10.1109/TAP.2007.902002.

[12] M. D. Gregory et al., "High-power metamaterial phase shifter using a relay-based approach," in *Proc. IEEE Int. Symp. Antennas Propag. (APSURSI)*, Fajardo, Puerto Rico, Jun./Jul. 2016, pp. 715–716.

[13] M. D. Gregory et al., "High power metasurface reflectarray antennas using switched shorted circular elements," in *Proc. IEEE Int. Symp. Antennas Propag. USNC/URSI Nat. Radio Sci. Meeting*, San Diego, CA, USA, Jul. 2017, pp. 1037–1038.

[14] X. Yang et al., "A broadband high-efficiency reconfigurable reflectarray antenna using mechanically rotational elements," *IEEE Trans. Antennas Propag.*, vol. 65, no. 8, pp. 3959–3966, Aug. 2017, doi: 10.1109/TAP.2017.2708079.

[15] S. M. A. Momeni Hasan Abadi, J. H. Booske, and N. Behdad, "MAcro-electro-mechanical systems (MÆMS) based concept for microwave beam steering in reflectarray antennas," *J. Appl. Phys.*, vol. 120, no. 5, 2016, Art. no. 054901, doi: 10.1063/1.4960352.

[16] X. Yang et al., "A mechanically reconfigurable reflectarray with slotted patches of tunable height," *IEEE Antennas Wireless Propag. Lett.*, vol. 17, no. 4, pp. 555–558, Apr. 2018, doi: 10.1109/LAWP.2018.2802701.

[17] M. U. Afzal, K. P. Esselle, and M. N. Y. Koli, "A beam-steering solution with highly transmitting hybrid metasurfaces and circularly polarized high-gain radial-line slot array antennas," *IEEE Trans. Antennas Propag.*, vol. 70, no. 1, pp. 365–377, Jan. 2022, doi: 10.1109/TAP.2021.3111522.

[18] K. Singh, M. U. Afzal, and K. P. Esselle, "Designing efficient phase-gradient metasurfaces for near-field meta-steering systems," *IEEE Access*, vol. 9, pp. 109080–109093, 2021, doi: 10.1109/ACCESS.2021.3100144.

[19] X. Zhao et al., "All-metal beam steering lens antenna for high power microwave applications," *IEEE Trans. Antennas Propag.*, vol. 65, 12, pp. 7340–7344, Dec. 2017, doi: 10.1109/TAP.2017.2760366.

[20] B. Ghassemiparvin and N. Ghalichechian, "Paraffin-based reconfigurable antenna operating at 100 GHz," *J. Microelectromech. Syst.*, vol. 29, no. 5, pp. 621–628, Oct. 2020, doi: 10.1109/JMEMS.2020.3013159.

[21] B. Ghassemiparvin and N. Ghalichechian, "Paraffin-based RF microsystems for millimeter-wave reconfigurable antenna," *IEEE Trans. Antennas Propag.*, vol. 70, no. 1, pp. 744–749, Jan. 2022, doi: 10.1109/TAP.2021.3102112.

[22] J. Eichenberger and N. Ghalichechian, "Mechanically reconfigurable slot array using accordion-like microactuators," *IEEE Antennas Wireless Propag. Lett.*, vol. 20, no. 10, pp. 2048–2052, Oct. 2021, doi: 10.1109/LAWP.2021.3102851.

[23] M. Lust, S. Chen, C. E. Wilson, J. Argo, V. Doan-Nguyen, and N. Ghalichechian, "High-contrast, highly textured VO_2 thin films integrated on silicon substrates using annealed Al_2O_3 buffer layers," *J. Appl. Phys.*, vol. 127, no. 20, 2020, Art. no. 205303, doi: 10.1063/1.5144816.

[24] S. Chen, M. Lust, and N. Ghalichechian, "Multiphysics simulation of hypersensitive microbolometer sensor using vanadium dioxide and air suspension for millimeter wave imaging," *Microsyst. Technol.*, vol. 27, no. 7, pp. 2815–2822, Jul. 2021, doi: 10.1007/s00542-020-05031-0.

[25] J. Ramsey, K. Henderson, and N. Ghalichechian, "Thermally actuated vanadium dioxide millimeter wave reflectarray," in *Proc. 16th Eur. Conf. Antennas Propag. (EuCAP)*, Madrid, Spain, Mar. 2022, pp. 1–4.

[26] K. Q. Henderson and N. Ghalichechian, "Circular-polarized metal-only reflectarray with multi-slot elements," *IEEE Trans. Antennas Propag.*, vol. 68, no. 9, pp. 6695–6703, Sep. 2020, doi: 10.1109/TAP.2020.2993229.

[27] K. Q. Henderson and N. Ghalichechian, "Triangular and rectangular lattices for cosecant-squared-shaped beam reflectarrays," *IEEE Antennas Wireless Propag. Lett.*, vol. 20, no. 10, pp. 2058–2062, Oct. 2021, doi: 10.1109/LAWP.2021.3103152.

[28] K. Q. Henderson and N. Ghalichechian, "Steerable reflectarray using tunable height dielectric for high-power applications," in *Proc. 14th Eur. Conf. Antennas Propag. (EuCAP)*, Copenhagen, Denmark, Mar. 2020, pp. 1–4.

[29] J. P. Gianvittorio and Y. Rahmat-Samii, "Reconfigurable patch antennas for steerable reflectarray applications," *IEEE Trans. Antennas Propag.*, vol. 54, no. 5, pp. 1388–1392, May 2006, doi: 10.1109/TAP.2006.874311.

[30] J. Rodriguez-Zamudio, J. I. Martinez-Lopez, J. Rodriguez-Cuevas, and A. E. Martynyuk, "Reconfigurable reflectarrays based on optimized spiraphase-type elements," *IEEE Trans. Antennas Propag.*, vol. 60, no. 4, pp. 1821–1830, Apr. 2012, doi: 10.1109/TAP.2012.2186231.

[31] A. E. Martynyuk, J. I. M. Lopez, and N. A. Martynyuk, "Spiraphase-type reflectarrays based on loaded ring slot resonators," *IEEE Trans. Antennas Propag.*, vol. 52, no. 1, pp. 142–153, Jan. 2004, doi: 10.1109/TAP.2003.820976.

[32] J.-M. Baracco, P. Ratajczak, P. Brachat, and G. Toso, "A dual frequency Ka-band printed Fresnel reflector for ground terminal applications," *IEEE Trans. Antennas Propag.*, vol. 63, no. 10, pp. 4352–4366, Oct. 2015, doi: 10.1109/TAP.2015.2456976.

[33] Y. He, C. Oakley, P. Chahal, J. Albrecht, and J. Papapolymerou, "Aerosol Jet printed 24 GHz end-fire quasi-Yagi-Uda antenna on a 3-D printed cavity substrate," in *Proc. Int. Workshop Antenna Technology: Small Antennas, Innov. Struct., Appl. (iWAT)*, Athens, Greece, 2017, pp. 179–182.

[34] A. C. Paolella, C. Corey, D. Foster, J. Desjardins, C. Smith, and L. Walters, "Broadband millimeter wave characterization of 3-D printed materials," in *IEEE MTT-S Int. Microw. Symp. Dig.*, Philadelphia, PA, USA, Jun. 2018, pp. 1565–1568.

[35] H. Yang et al., "A study of phase quantization effects for reconfigurable reflectarray antennas," *IEEE Antennas Wireless Propag. Lett.*, vol. 16, pp. 302–305, 2017, doi: 10.1109/LAWP.2016.2574118.

Walter Disharoon (Graduate Student Member, IEEE) received the B.S. degree in electrical engineering from Kennesaw State University, Kennesaw, GA, USA, in 2021. He is currently pursuing the Ph.D. degree with the mmWave Antennas and Arrays Laboratory, Georgia Institute of Technology, Atlanta, GA, USA.

He did a co-op at the Georgia Tech Research Institute with a focus in RF engineering, digital arrays, field programmable gate array (FPGA) development, and automated RF measurements. His research interests include reconfigurable metasurfaces, antennas, and reconfigurable devices enabled by vanadium dioxide.

Nima Ghalichechian (Senior Member, IEEE) received the B.S. degree in electrical engineering from the Amirkabir University of Technology, Tehran, Iran, in 2001, and the M.S. and Ph.D. degrees in electrical engineering from the University of Maryland-College Park, College Park, MD, USA, in 2005 and 2007, respectively.

He is an Assistant Professor at the School of Electrical and Computer Engineering, Georgia Institute of Technology, Atlanta, GA, USA. Prior to joining Georgia Tech in 2021, he was an Assistant Professor at The Ohio State University (OSU), Columbus, OH, USA, from 2017 to 2021. From 2007 to 2012, he was with the Research Department, FormFactor Inc., Livermore, CA, USA, as a Senior Principal Engineer. He was a Research Scientist and a Research Assistant Professor at OSU from 2012 to 2017. He is the Director of the mmWave Antennas and Arrays Laboratory at Georgia Institute of Technology. He is currently an Associate Director of the Georgia Electronic Design Center (GEDC), Atlanta, GA. His research area is mmWave antennas and arrays.

Dr. Ghalichechian was a recipient of the College of Engineering Lumley Research Award at OSU in 2018, the NSF CAREER Award in 2019, the U.S. Air Force Faculty Summer Fellowship Award in 2019, and the ECE Excellence in Teaching Award at OSU in 2020. He is an Associate Editor of the IEEE TRANSACTIONS ON ANTENNAS AND PROPAGATION and the IEEE ANTENNAS AND WIRELESS PROPAGATION LETTERS.

Kendrick Q. Henderson (Member, IEEE) received the B.S. degree in electrical engineering, the B.S. degree in computer engineering, and the M.S. degree in electrical engineering from the University of South Alabama, Mobile, AL, USA, in 2015, 2015, and 2017, respectively, and the Ph.D. degree from the ElectroScience Laboratory, Department of Electrical and Computer Engineering, The Ohio State University, Columbus, OH, USA, in 2021.

He has been at the Radar Division, Naval Surface Warfare Center–Crane, Crane, IN, USA, as an Antenna Engineer, since 2021. He has authored 16 conference papers and four journal articles in the field of antennas and electromagnetics throughout his time as a Researcher. His research interests include reflectarrays, metasurfaces, phased arrays, and waveguide-based antennas.